REVIEW ARTICLE

Numerical simulation of manufacturing process chain for pearlitic and bainitic steel rails

Andrij Milenin[1] · Władysław Zalecki[2] · Monika Pernach[1] · Łukasz Rauch[1] · Roman Kuziak[2] · Tomasz Zygmunt[3] · Maciej Pietrzyk[1]

Abstract

Computer system for the design of technology of the manufacturing of pearlitic and bainitic rails was presented in this paper. The system consists of the FEM simulation module of thermal–mechanical phenomena and microstructure evolution during hot rolling integrated with the module of phase transformation occurring during cooling. Model parameters were identified based on dilatometric tests. Physical simulations, including Gleeble tests, were used for validation and verification of the models. In the case of pearlitic steels, the process of subsequent immersions of the rail head in the polymer solution was numerically simulated. The objective function in the optimization procedure was composed of minimum interlamellar spacing and maximum hardness. Cooling in the air at a cooling bed was simulated for the bainitic steel rails and mechanical properties were predicted. The obtained results allowed us to formulate technological guidelines for the process of accelerated cooling of rails.

✉ Monika Pernach
pernach@agh.edu.pl

Andrij Milenin
milenin@agh.edu.pl

Władysław Zalecki
wzalecki@imz.pl

Łukasz Rauch
lrauch@agh.edu.pl

Roman Kuziak
RKuziak@imz.pl

Tomasz Zygmunt
Tomasz.Zygmunt@arcelormittal.com

Maciej Pietrzyk
mpietrz@agh.edu.pl

[1] AGH University of Science and Technology, al. Mickiewicza 30, 30-059 Kraków, Poland

[2] Institute for Ferrous Metallurgy, ul. K. Miarki 12, 44-100 Gliwice, Poland

[3] ArcelorMittal Poland, al. Józefa Piłsudskiego 92, 41-308 Dąbrowa Górnicza, Poland

1 Introduction

There is a continuous need to improve the mechanical properties of rails used extensively in the railway transportation sector. The extent of improvement in these rails is known to be governed by factors like wear resistance, fatigue strength, etc. These properties are in turn dependent on microstructuraol constituents and their morphology. Properties of pearlitic rails are strongly dependent on the interlamellar spacing and the fraction of cementite within the pearlite. Experimental tests [1] have shown that the structure of fine pearlite, obtained by lowering the transformation temperature, increases significantly the hardness of the pearlitic steels.

The even greater degree of microstructure refinement can be achieved by transforming steels having complex chemical composition to bainite [2, 3]. The final microstructure of rails is obtained by precise control of parameters of the whole manufacturing chain including multi-pass hot rolling and heat treatment. These parameters can be determined by numerical models. The development of the finite element (FE) thermal–mechanical-metallurgical model of the manufacturing chain for rails was the objective of this work.

Numerical models of rolling and cooling are usually non-integrated [4, 5]. 3D solutions for metal flow were

time-consuming 20 years ago, therefore, researchers have searched for the simplified approach, which allowed maintaining the accuracy of simulation at a reasonable level. In the mechanical part, so called generalized plane-strain approach (2.5D) appeared to be very efficient [6]. This approach simplified the strain and strain rate tensors and significantly saved computing time without noticeable decreasing accuracy of the solution. The main assumption of that model is the decomposition of the process into several steps related to subsequent material locations in the roll gap. It was assumed that the strain tensor components assigned to the rolling direction are distributed uniformly across the rail cross-section, which is perpendicular to the rolling axis. This assumption results in constant strains and strain rates in the rolling direction and it reduced shear components of strain and strain rate tensors related to that direction. Only a cross-section of the rail was analyzed using a non-steady state approach keeping in mind that the whole process is spatial. In the thermal part of the model, the 2.5D assumption led to neglecting the conduction along the rail. The 2.5D approach was combined with the microstructure evolution model [7] and became a very efficient tool for simulations of rail rolling [8]. Another simplified approach was used in [9] to calculate residual stresses in rails.

New generation computers allow full 3D modelling of rail rolling and there are several papers published showing this solution, the examples may be seen in [10–12], but it is still computationally expensive. Therefore, when only forces were to be calculated simplified models or artificial intelligence methods were used [13]. Over the last years much more attention, however, has been paid to the cooling process, what is because the final microstructure and properties of rails are determined in this process. The problem of heat treatment of rails directly after hot rolling has been thoroughly analyzed. Numerous papers dealing with the phenomena of heat transfer [14], wear resistance [15], microstructure evolution [15, 16], and thermal stresses [17] can be found in the scientific literature. Recent research is focused on searching for a direct connection between cooling process parameters and wear resistance of rails [18]. Detailed analysis of published research shows that rolling and cooling processes are treated separately. Thus, the development and validation of the model of the whole manufacturing chain for rails is the general objective of the present paper.

The focus of the current research is on the model, which connects rolling and cooling processes and which can predict microstructure evolution and phase transformation kinetics during the production of rails. Two types of steels, pearlitic and bainitic, were investigated. Phase transformation models for pearlitic steel were developed in earlier publications [19, 20] and only main equations are repeated here for completeness of this paper. All material models for bainitic rail steel were developed in the present work and are described below.

Identification and verification of the models were performed based on a series of experiments. Evaluation of the possibility of using numerical simulations to design the manufacturing process, and as consequence improvement properties of products was the general objective of this paper.

2 Models

2.1 Finite element model for hot rolling and cooling

Qform FE software was used in hot rolling simulations. This software is based on flow formulation as proposed in [21] coupled with the solution of the heat transfer equation. Flow stress was described by:

$$\sigma_p = K\varepsilon^p \exp(-q\varepsilon)\dot{\varepsilon}^m \exp(-\beta T) \tag{1}$$

where ε is the strain, $\dot{\varepsilon}$ is strain rate, T is the temperature in °C, K, p, q, m, β are coefficients.

The problems of rigid-plastic non-isothermal deformation of the material during passes and its cooling between subsequent passes is considered. At all stages of the calculation, a full three-dimensional model of the deformable workpiece and calibers was considered. 17 passages and 18 cooling steps during pauses between passes were considered (the first cooling step begins before the first pass after the material leaves the heating furnace). The results of the solution in the current pass (temperature and accumulated strain) are transferred to the next stage of the calculation in the form of values at the nodes of the FE mesh. The time pause between passes varied following the speed of movement of the workpiece and the time interval from 39 s (pause before the first pass) to 1.65 s (pause before the last pass). The rotation speeds of the rolls were set by the used technology and corresponded to the rolling speeds at various stages of the technology from 1.7 to 6.7 m/s. The first seven passes were carried out in a reversing stand. The full length of the workpiece was considered in this case during FE modelling. However, when FE simulation of the following passes was carried out, a sufficiently long section of the billet was considered, which made it possible to obtain a solution for both the unsteady rolling stage and the stationary one.

In modeling the processes described above, three-dimensional tetrahedral FEs were used. When simulating cooling during pauses, the FE grid remained constant over each time interval. The number of FEs and grid nodes varied from 51,856 and 12,735, respectively, during the first pause to 345,674 and 78,541, respectively, during the last pause. Such a significant change in the number of nodes and elements is associated with a complicated geometry of the section in the last passes. The minimum FE size also was changed at different stages of technology. Before the

first pass, it was 10 mm, and during the simulation of the last pass, it was 2 mm. These values are approximate since Qform uses complex algorithms for automatic adaptation of the FE grid at each time step of the solution. The maximum size of elements was determined by Qform algorithm for mesh adaptation.

During the simulation of the rolling pass, the FE grid was remeshed according to the criteria of the complexity of the profile shape and the distortion of the shape of the FE elements during deformation. This allowed at each step of the calculation to have a FEs shape close to the shape of a regular tetrahedron, which limits a high numerical error. For this reason, when modeling passes, the number of nodes and FE elements was not constant. The FE mesh obtained in the last step of the rolling pass was transferred to the stage of modeling of subsequent cooling pause. After the completion of the cooling simulation, a virtual cutting of the workpiece was carried out, and the resulting mesh was transferred to the next pass. After modeling the last pause, corresponding to the time the rails completely exited the rolls (this time was 2 s), the obtained distributions of temperature, effective strain, and grain diameter in the cross-section of the profile was transferred to another FE program, which performed 2D modeling of cooling of the rail and related structural transformations.

FE program described in [22] was used to simulate the cooling of rails after rolling. Microstructure evolution and mechanical properties models, which are described in the following sections, were implemented in the FE codes.

2.2 Microstructure evolution

Recrystallization and grain size were described by equations formulated based on the works of Sellars [23]. The kinetics of phase transformations is described by the JMAK (Johnson–Mehl–Avrami-Kolmogorov) model:

$$X = 1 - \exp\left(-kt^n\right) \tag{2}$$

where X is the volume fraction of a new phase, t is time, k, n are coefficients.

Sellars related time in equation (2) to the time for 50% of recrystallization ($t_{0.5}$), what gave $k = \ln(0.5)$. Remaining equations of the microstructure evolution model are given in The microstructure of rails after hot rolling, which is crucial for phase transformations kinetics, is determined in the last few passes. Since static recrystallization dominates during these passes, metadynamic recrystallization was neglected in the model. The flow chart of calculations in of the microstructure evolution is shown in Fig. 1. Following the chart, this model was implemented into the Qform FE program. To do this, LUA scripts were developed. The equations in Table 1 were transferred to the incremental form. As a result, the distributions of all the parameters from Table 1 were obtained for each time step.

Table 1, where Z is Zener–Hollomon parameter, $t_{0.95}$ is time for 95% of recrystallization, which is considered the total time of recrystallization, ε_s is saturation strain, D_0 is grain size before deformation, T is the temperature in K. The microstructure evolution model contains several coefficients,

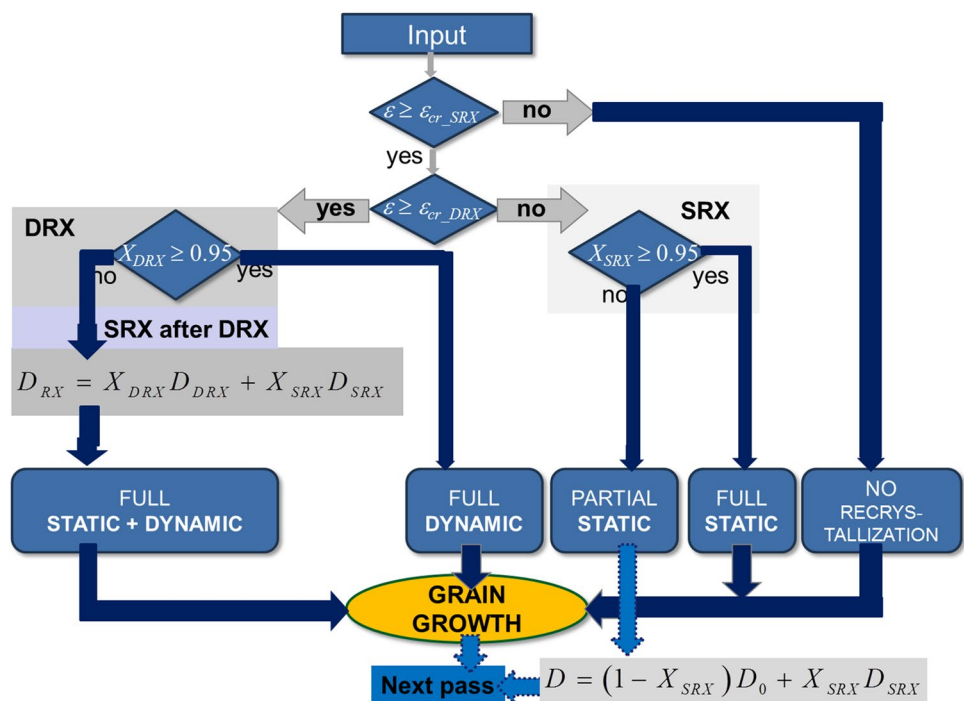**Fig. 1** The flow of calculations in the microstructure evolution model

Table 1 Equations in the microstructure evolution model

Time for 50% recrystallization	$t_{0.50} = A\varepsilon^{-a_1}\dot{\varepsilon}^{a_2}D_0^{a_3}\exp\left(\frac{Q_{SRX}}{RT}\right)$
Grain size after SRX	$D_{SRX} = B\varepsilon^{-b_1}\dot{\varepsilon}^{-b_2}D_0^{b_3}\exp\left(\frac{-Q_{DSRX}}{RT}\right)$
Time of SRX	$t_{SRX} = t_{0.95} = \left[\frac{\ln(0.05)}{\ln(0.5)}\right]^{\frac{1}{n}}$ $t_{0.95} = 4.3219^{\frac{1}{n}}t_{0.50}$
Critical strain for DRX	$\varepsilon_{cr\_DRX} = p_1 D_0^{p_2} Z^{p_3}$
DRX volume fraction	$X_{DRX} = 1 - \exp\left[-p_7\left(\frac{\varepsilon-\varepsilon_{cr\_DRX}}{\varepsilon_s-\varepsilon_{cr\_DRX}}\right)^{p_8}\right]$
Saturation strain	$\varepsilon_s = p_4 D_0^{p_5} Z^{p_6}$
Grain size after DRX	$D_{DRX} = p_9 Z^{-p_{10}}$
Grain growth	$D_t^s = D_{RX}^s + Kt\exp\left(-\frac{Q_{GROWTH}}{RT}\right)$

which were determined based on stress relaxation tests (static recrystallization—SRX) and analysis of the flow curves (dynamic recrystallization—DRX).

The microstructure of rails after hot rolling, which is crucial for phase transformations kinetics, is determined in the last few passes. Since static recrystallization dominates during these passes, metadynamic recrystallization was neglected in the model. The flow chart of calculations in of the microstructure evolution is shown in Fig. 1. Following the chart, this model was implemented into the Qform FE program. To do this, LUA scripts were developed. The equations in **Table 1** were transferred to the incremental form. As a result, the distributions of all the parameters from Table 1 were obtained for each time step.

2.3 Phase transformations

Model of phase transformation was based on the JMAK (Johnson–Mehl–Avrami–Kolmogorov) equation (2) with the following upgrades:

- Coefficient n was identified based on dilatometric tests and takes constant values a_4, a_{16}, and a_{24} for ferrite, pearlite, and bainite transformations, respectively.
- According to [24, 25] coefficient k is temperature-dependent and is described by equations given in Table 2.
- Using Gauss function for k_f does not require accounting for the incubation time. It is assumed that ferrite transformation begins when 5% of ferrite is predicted.
- Calculations of carbon concentration in the austenite during both ferrite and bainite transformations were added and prediction of the retained austenite became possible.
- The T_0 temperature concept proposed in [26] was added for the bainitic steel.
- Equations describing current carbon content in the austenite ($c\gamma$), temperatures of bainite start (B_s) and martensite start (M_s), as well as martensite volume fraction (F_m) are shown in Table 2, where F_f, F_p and F_b are volume fractions of ferrite, pearlite, and bainite, respectively, p represents the probability that a new platelet of the bainitic ferrite forms in a close neighbourhood of the existing one, what constrains its diffusion field [27]. The

Table 2 Relations describing incubation time (τ) and coefficient (k) in the equation (2) used in the phase transformations model

Ferrite	Pearlite	Bainite
–	$\tau_P = \frac{a_9}{(A_{e1}-T)^{a_{11}}}\exp\left(\frac{a_{10}}{RT}\right)$	$\tau_b = \frac{a_{17}}{(B_s-T)^{a_{19}}}\exp\left(\frac{a_{18}}{RT}\right)$
$k_f = \frac{a_5}{D_\gamma}\exp\left[-\left(\frac{|T-T_{nose}|}{a_7}\right)^{a_8}\right]$	$k_p = \frac{a_{14}}{D_\gamma^{a_{16}}}\exp\left(a_{13}-a_{12}\frac{T}{100}\right)$	$k_b = a_{23}\exp\left[-\left(\frac{T-a_{21}}{a_{22}}\right)^2\right]$
$T_{nose} = A_{e3} - \frac{400}{D_\gamma} + a_6$		
$c_\gamma = \frac{\left[c_0-\left(F_f+\frac{F_b}{1-p}\right)c_\alpha\right]}{1-F_f-\frac{F_b}{1-p}}$		
$B_s = a_{20} - 425[C] - 42.5[Mn] - 31.5[Ni]$		
$M_s = a_{25} - a_{26}c_\gamma$	$F_m = (1-F_f-F_p-F_b)\left\{1-\exp\left[-0.011(M_s-T)\right]\right\}$	

numerical solution of the present model is described in [28].

The heat generated during transformation per unit volume is calculated as:

$$\dot{Q} = \Delta H \rho \frac{dF}{dt} \tag{11}$$

where ΔH is the enthalpy of the transformation, ρ is density, F is the volume fraction of the considered structural component.

Enthalpy of the transformations was determined using ThermoCalc software and it was $\Delta H = 11$ kJ/kg for bainite transformation and $\Delta H = 182 - 0.15$ T. The values of microstructural parameters having a crucial influence on the mechanical properties of pearlitic steel, i.e., interlamellar spacing (S_0), pearlite colony size (D_c) and pearlite grain size (D_p) were calculated based on the following relationships [19]:

$$S_0 = \frac{1}{a - bT_p} \tag{12}$$

$$D_c = \frac{1}{0.857 - 0.00119T_p} \tag{13}$$

$$D_p = \frac{6500 \left[1 - \exp\left(-0.016 D_\gamma \right) \right]^{0.6}}{\text{Ae}_1 - T_p} \tag{14}$$

where T_p is a weighted average temperature of the pearlite transformation calculated as:

$$T_p = \frac{1}{F_p} \int_0^{F_p} T dF_p \tag{15}$$

and F_p is pearlite volume fraction.

In the case of bainitic steel phase composition, including volume fraction of the retained austenite, at the rail cross-section was crucial for the prediction of the mechanical properties.

2.4 Mechanical properties

The mechanical properties of the pearlitic rail steel with fine interlamellar spacing are determined as [19]:

$$\sigma_y = 295.5 + 114.2\chi^{-1}$$
$$\text{UTS} = 672.5 + 99.4\chi^{-1} + 72[\text{Si}] \tag{16}$$

where $\chi = (2S_0 - t)$ is the mean free path for dislocation glide in pearlitic ferrite and t is thickness of the cementite plate calculated as $0.015S_0$[C].

Equation describing the the hardness of the pearlite was obtained by approximation of the experimental data:

$$HV_p = c + \frac{d}{S_0} \tag{17}$$

Following the RFCS project [29], the yield stress of bainitic steel was a linear sum of strength of pure annealed iron (σ_{Fe}), substitutional solid solution strengthening (σ_{SS}), and a variety of microstructural components including dislocation strengthening (σ_ρ), precipitation strengthening (σ_{pp}) and grain size effect (σ_{GS}). In the case of Nb and Ti steels, the yield strength is a sum obeying a Pythagorean law was used:

$$\sigma_y = \sigma_{\text{FE}} + \sigma_{\text{SS}} + \sigma_{\text{GS}} + \sqrt{\sigma_\rho^2 + \sigma_{\text{pp}}^2} \tag{18}$$

The strength of ferritic iron was estimated to be 85–88 MPa [30]. Empirical relation was used to consider the influence of alloying on the solid solution strengthening:

$$\sigma_{\text{SS}} = \sum A_i \text{wt\%}_i \tag{19}$$

where A_i is a factor for strengthening resulting from wt% equal to 32, 84, 38, 33, 54, 11, and 30 for Mn, Si, Cu, Ni, Cr, Mo, and Al, respectively [29].

The bainite grain size contribution assumes that, rather than $d^{-1/2}$ Hall–Petch type relationship, the strength is related to reciprocal of some characteristic scale [29]:

$$\sigma_{\text{GS}} = \sigma_0 + k_y D_b^{-1} \tag{20}$$

where D_b is bainite grain size, $\sigma_0 = 100$ MPa [30] is friction stress, $k_y = 551$ MPa·μm [31] is the grain boundary resistance.

As proposed in [32], the bainite grain relation on the prior austenite grain size (D_γ) is:

$$D_b = 1.4 D_\gamma^{0.55} \tag{21}$$

The precipitation strengthening depends on the following factors: nature of interaction of precipitates with dislocations, the volume fraction, and the size of particles. Since quantitative evaluation of the contribution of each factor is difficult, an alternative method to estimate the precipitation strengthening in Nb-Ti steels was used, as follows:

$$\sigma_{\text{pp}} = \frac{2MGb}{d} \sqrt{\frac{f}{\pi}} \left(\frac{F}{Gb^2} \right)^{\frac{3}{2}} \tag{22}$$

where M is the Taylor factor, G is shear modulus, b is the Burger vector, d, f are the size and volume fraction of

precipitates, respectively, F is resistance force of the second phase particle.

Contribution of the dislocation density is due to motion and production of dislocations:

$$\sigma_\rho = \beta G b \sqrt{\rho} \tag{23}$$

where $\beta = 0.38$ [33] is coefficient, ρ is average dislocation density, which depends on the bainite transformation temperature (T_b) according to the equation [34]:

$$\log(\rho) = 9.2848 + \frac{6880}{T_b} + \frac{1780360}{T_b^2} \tag{24}$$

An ultimate tensile stress was calculated as $UTS = \alpha\sigma_y$ and $\alpha = 1.69$ was determined by approximation of experimental results. Elongation of bainitic steel was calculated as:

$$A_5 = 28.3 - 22.4[C] - 3.6[Mn] + 0.5[Si] - 0.09[Cr] \\ + 10.4[Ni] - 10.4[Mo] - 1299[B] \tag{25}$$

Equations describing the microstructure and properties of the investigated steels were solved at the stage of post-processing in each Gauss integration point of the FE mesh. In consequence, the distribution of the properties at the rail cross-section could be calculated. The phase transformation model was fully coupled with the FE code, which means that the rate of the heat generated during transformation was calculated from the equation (11) and it was accounted for in the FE solution of the heat transfer equation. Due to the full coupling of the micro scale models, distribution of the microstructural parameters and properties at the rail cross-section could be calculated.

3 Experiments—identification of models

Three grades of steel used for the manufacturing of rails were investigated. The first was typical pearlitic steel containing 0.7%C and 1.1%Mn. This steel was thoroughly investigated in [20]. Remaining two were bainitic steels containing 0.33% C and 1.43% Mn distinguished by the concentration of chromium. Steel A with 1.49% Cr and steel B with 0.8% Cr. Three types of tests were performed, plastometric tests for identification of the flow stress model, stress relaxation tests for identification of the microstructure evolution model, and dilatometric tests for identification of the phase transformation model. Beyond this, physical simulations of cooling of rails were performed to supply data for validation and verification of the models.

3.1 Compression tests—flow stress

Uniaxial compression tests were performed to supply data for the identification of the flow stress models for. Samples

measuring $\phi 5 \times 12$ mm were compressed in the temperatures 800–1200 °C and with the strain rates of 0.1, 1, and 10 s^{-1}. All samples were preheated at 1210 °C for 60 s, cooled to the test temperature with the rate of 2 °C/s, maintained at this temperature for 5 s and compressed. Inverse approach [35] was applied for interpretation of the tests and the results are given in Table 3. Similar results were obtained for both bainitic steels. Figure 2 shows selected comparisons of the flow stress for pearlitic and bainitic steels. It is seen that the level of the flow stress is comparable but the critical strain for the DRX is lower for the bainitic steel.

3.2 Microstructure evolution

Stress relaxation tests were performed to identify coefficients in the static recrystallization model. The identification of the dynamic recrystallization model was performed based on the flow curves presented in the previous section. Coefficients in the microstructure evolution model for both steels are given in Table 4 for static recrystallization and in Table 5 for dynamic recrystallization. The activation energy in the Zener-Hollomon parameter is 315,000 J/molK and 270,960 J/molK for pearlitic and bainitic steels, respectively.

3.3 Phase transformations

Coefficients used in the model of phase transformation were identified based on dilatometric tests. Results of the model identification for pearlitic steel are described in [20]. Bainitic steel samples were subjected to thermomechanical cycle shown in Fig. 3. Coefficients in the phase transformation model are given in Table 6 for the steel A and in Table 7 for the steel B. Models were validated for various cooling rates and reasonably good accuracy of the model was confirmed. Results may be seen in [20] for the pearlitic steel and in Fig. 4 for the bainitic steels.

Several experiments were performed in [20] to supply data for identification of the coefficients in the equation (12) describing interlamellar spacing in the pearlitic steel. The experiments on the dilatometer composed isothermal tests at the temperatures of 520, 550, 600, and 650 °C and constant cooling rate tests with the rates of 0.25, 0.5, 1, 2, 5, and 10 °C/s. Microstructure was analyzed after each test and interlamellar spacing was measured. Combination of the measurements with calculated average transformation temperature using equation (15) allowed to determine

Table 3 Coefficients in equation (1) determined using inverse analysis for both steels

Steel	K	p	q	M	β
Pearlitic	3547.4	0.3534	0.905	0.149	0.00266
Bainitic	4386.7	0.276	0.3855	0.1397	0.003256

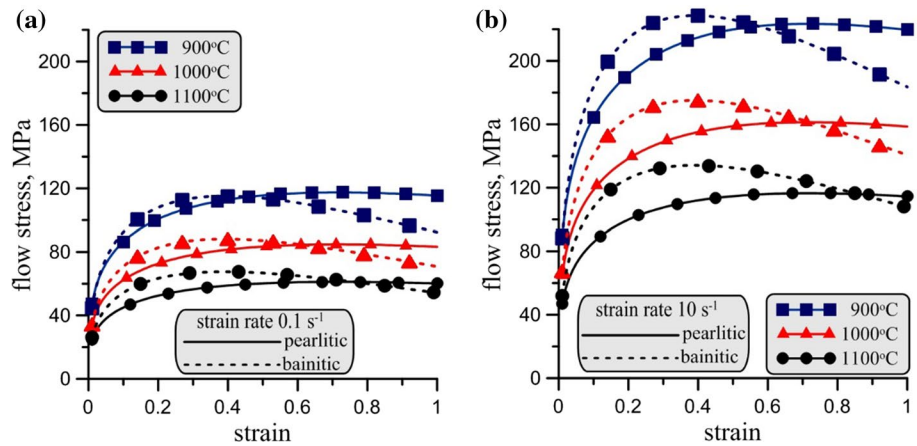**Fig. 2** Flow curves for the investigated steels at strain rates of 0.1 (**a**) and 10 s^{-1} (**b**)

Table 4 Coefficients in the static recrystallization model for pearlitic and bainitic steels

Steel	n	A	a_1	a_2	a_3	Q_{SRX}	B	b_1	b_2	b_3	Q_{DSRX}
Pearlitic	1.82	7.42×10^{-11}	−0.786	0.53	2	100,000	9.91	−0.386	−0.1	0.444	17,540
Bainitic	0.71	6.6×10^{-8}	−0.676	0.53	2.608	50,159	304	0.65	−0.048	0.54	47,183

Table 5 Coefficients in the dynamic recrystallization model for pearlitic and bainitic steels

Steel	p_1	p_2	p_3	p_4	p_5	p_6	p_7	p_8	p_9	p_{10}
Pearlitic	5.0562×10^{-4}	0.15	0.0088	2.809×10^{-4}	0.26	0.36187	4.60517	1.5	16,000	0.23
Bainitic	2.23×10^{-3}	0.1315	0.188	7.1×10^{-4}	0.05	0.2856	1.443	1.94	733.4	0.129
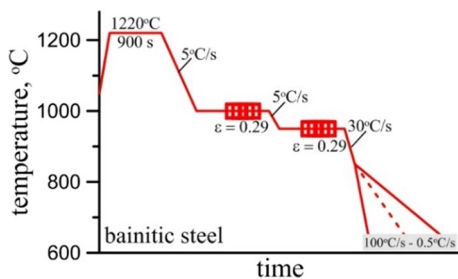
Fig. 3 Thermomechanical cycle preceding dilatometric tests for bainitic steels

coefficients in equation (12): $a = 28.8$; $b = 0.0318$. Measured and calculated interlamellar spacing is presented in [20] where good agreement was confirmed. Coefficients in equation (17) were determined based on experimental tests

carried out on the Gleeble 3800 simulator and the following values were obtained: $c = 273$; $d = 12.2$. The verification of this model is presented in Fig. 5.

The whole model describing microstructural parameters and mechanical properties for the pearlitic steels was implemented in the FE code for cooling of rails, and optimization of this process was performed.

4 Experiments—validation and verification of the models

4.1 Pearlitic steel

The main goal of the heat treatment of high-strength rails is to obtain the structure of fine pearlite. Research presented in [1] shows a significant reduction of the interlamellar spacing

Table 6 Coefficients in the phase transformation model for bainitic steel A

a_4	a_5	a_6	a_7	a_8	a_9	a_{10}	a_{11}	a_{12}	a_{13}	a_{14}	a_{15}
0.978	0.464	115.2	8.981	1.0	3.402	35.31	0.0053	0	0	0	0.0003

a_{16}	a_{17}	a_{18}	a_{19}	a_{20}	a_{21}	a_{22}	a_{23}	a_{24}	a_{25}	a_{26}	a_{27}
1.1	56.41	56.37	1.826	782.5	436.6	20.0	0.483	0.634	374.2	218.2	0.004

Table 7 Coefficients in the phase transformation model for bainitic steel B

a_4	a_5	a_6	a_7	a_8	a_9	a_{10}	a_{11}	a_{12}	a_{13}	a_{14}	a_{15}
0.978	0.464	115.2	8.981	1.0	3.402	35.31	0.0053	0	0	0	0.0003

a_{16}	a_{17}	a_{18}	a_{19}	a_{20}	a_{21}	a_{22}	a_{23}	a_{24}	a_{25}	a_{26}	a_{27}
1.1	56.41	56.37	1.826	782.5	436.6	20.0	0.483	0.634	374.2	218.2	0.004

Fig. 4 Comparison of measured (full symbols) and calculated (open symbols with lines) start and end temperatures of phase transformations for bainitic (b) steels
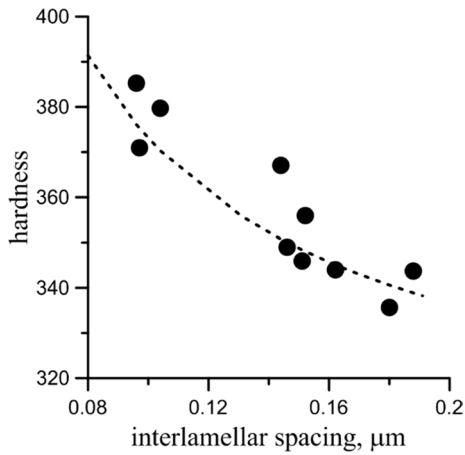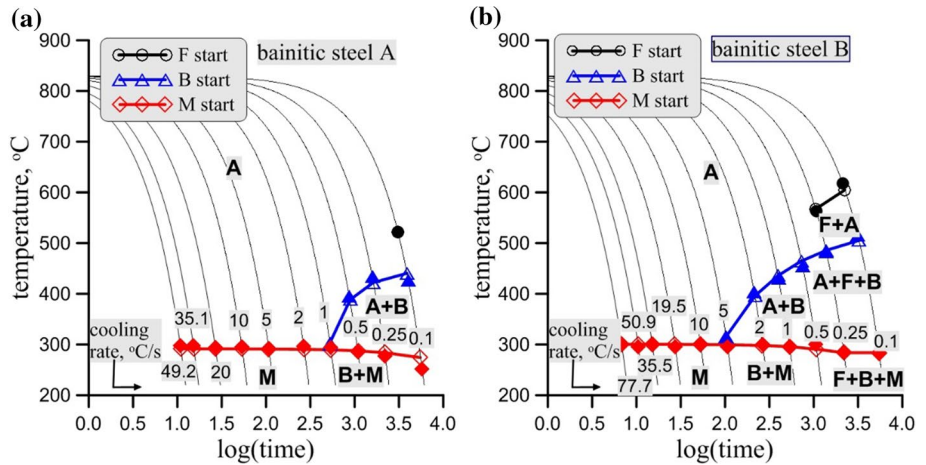
Fig. 5 Comparison of measured (full symbols) and calculated from the equation (17) with optimal coefficients (dashed line) hardness in the Gleeble tests

and the pearlite colony size during hardening of rail head by cyclic immersion in aqueous polymer solutions, as compared to these parameters after cooling in still air. This process, described also in [16], consists of subsequent immersions of the rail head in the solution. As a consequence, a low average temperature of the pearlite transformation can be obtained and the bainite can be avoided. Modelling of this process requires the identification of the heat transfer coefficient for cooling in the solution. This coefficient can be changed by

changing polymer concentration. Laboratory experiments of cooling of rail with three thermocouples inserted at its cross-section were performed. The concentration of the polymer was 5%. Locations of the thermocouples were 2 mm (A), 6 mm (B), and 18 mm (C) below the surface of the head. The rail was cooled in the air to 850 °C and then immersed in the solution for 80 s. Following this, eight cycles composed of 10 s in the air and 5 s in the solution were applied. The following heat transfer coefficient was determined by inverse analysis of all experimental data: 1700 W/m^{2}K for temperatures exceeding 700 °C, increasing below this temperature and reaching 2400 W/m^{2}K at 300 °C, decreasing below this temperature to 1200 W/m^{2}K at the ambient temperature. An example of the comparison of measured and calculated temperatures for eight immersions is presented in Fig. 6. The model predicts temperatures reasonably well, although oscillations of the temperature close to the surface were smoothed by the inertia of thermocouples. Similar results were obtained for the remaining tests.

Developed models of phase transformations allow the complex description of both phase composition of eutectoid steels as well as morphological parameters of structural components defined in Sections 0–0, including such specific features of the perlite as pearlite grain size, colony size, and interlamellar spacing. The phase transformation model and mechanical properties model were validated and verified in [20] and their good predictive capabilities were confirmed.

4.2 Bainitic steel

Physical and numerical simulations of thermal cycles in Fig. 7a were performed for the bainitic steel. Tests were carried out for various holding temperatures (T_h), while the holding time was 900 s in all cases. The main goal was to evaluate the model's capability to predict the occurrence of the retained austenite (RA). Experimental verification (Fig. 7b) shows that the model correctly describes the kinetics of phase transformations, include volume fraction of RA. Very good qualitative agreement and reasonable quantitative agreement between measurements and calculations was obtained, although larger discrepancies were observed in few tests.

Microstructures of the samples are presented in Fig. 8. Degenerated bainite with martensite islands and some retained austenite was observed in the samples after holding temperatures 380–450 °C. The smallest amount of the martensite was obtained for $T_h = 400$ °C. Cycle with $T_h = 480$ °C resulted in lower bainite with martensite and it is not presented here.
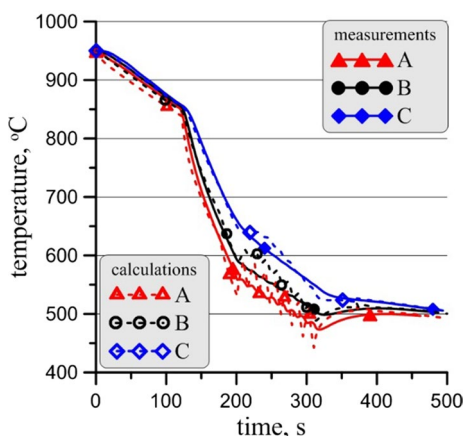
Fig. 6 Comparison of measured (solid lines) and calculated (dashed lines) temperatures at the three locations
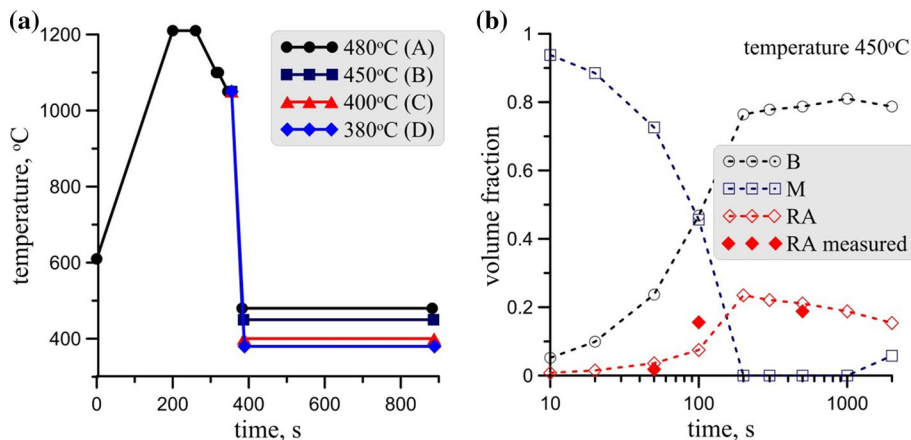
The microstructure of the samples after holding consists mainly of degenerated upper bainite with blocks of martensite, however, the volume fraction of martensite is limited to max. 10%. The degree of refinement of the microstructure increases as the holding temperature decreases.

5 Simulation and optimization of the manufacturing chain for rails
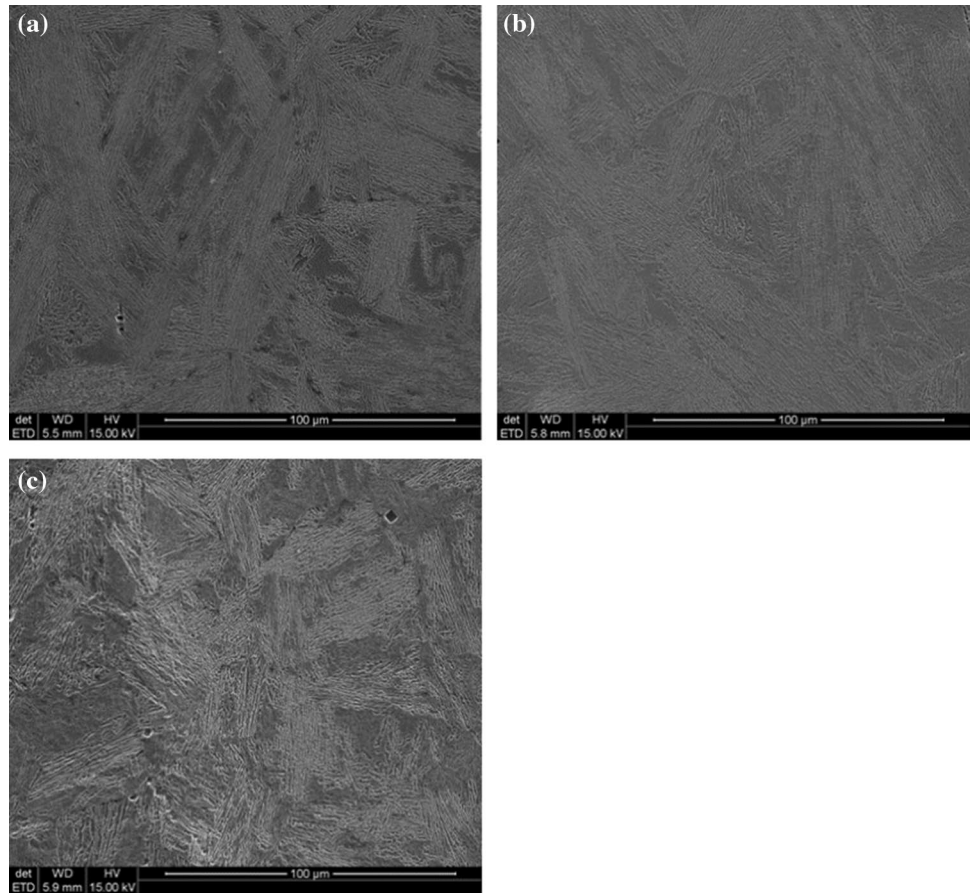
5.1 Rolling

A typical rolling mill for rails was considered. Simulations of the hot rolling process were carried out using Qform FE software and the selected results for both steels are shown below.

The difference in temperature and strains distribution between pearlitic and bainitic steels is small. Contrary, the microstructure evolution is noticeably different, due to high-temperature dynamic recrystallization dominated in the break down passes for both steels. Figures 9 and 10 shows distributions of the critical strain and dynamically recrystallized volume fraction in the 3rd pass for pearlitic and bainitic steels, respectively. Results show that DRX was completed for the pearlitic steel (Fig. 9b) while in bainitic steel only a small volume of metal recrystallized according to dynamic mechanism (Fig. 10b).

In the last pass, no 17, partial dynamic recrystallization for the pearlitic steel was observed, but the dominant mechanism of recrystallization was static. For bainitic steel, the value of the critical strain was greater than the value of the effective strain and dynamic recrystallization did not start. Static recrystallization only was observed (Fig. 11).

Modelling of the mechanisms of recrystallization (dynamic and static) showed that for pearlitic steel the recrystallization rate is larger than for bainitic steel. However, during 1.5 s after the last pass, the recrystallization of both steels was completed.

Fig. 7 Investigated thermal cycles (**a**) and predictions of phase volume fractions compared to the measurements of the RA volume fraction in cycle B (**b**) for the bainitic steel

Fig. 8 Microstructures of the bainitic steel after thermal cycles in Fig. 7, holding temperature 380 °C (**a**), 400 °C (**b**), and 450 °C (**c**)

Finally, distributions of temperature and grain size at the rail cross-section after the rolling process were determined (Fig. 12). The results show that pearlitic steel has larger grains than bainitic steel. The distribution of grain diameter is more uniform for bainitic steel. These data were a starting point for further simulation of phase transformations during cooling.

6 Heat treatment

6.1 Pearlitic steels—effect of the end of rolling temperature

The process of controlled cooling of rails was simulated using the FE program [36] with phase transformation and
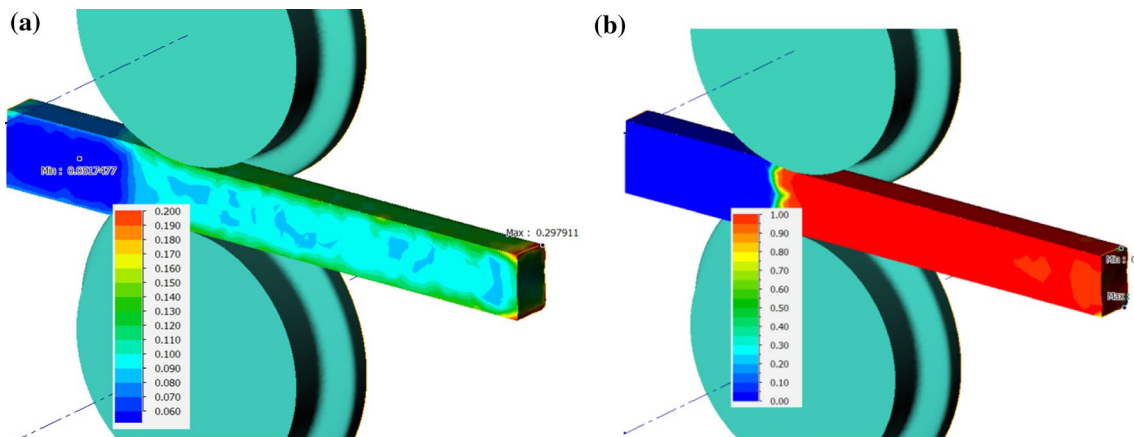
Fig. 9 Distribution of the critical strain (**a**) and recrystallized volume fraction (**b**) in the 3rd pass for the pearlitic steel
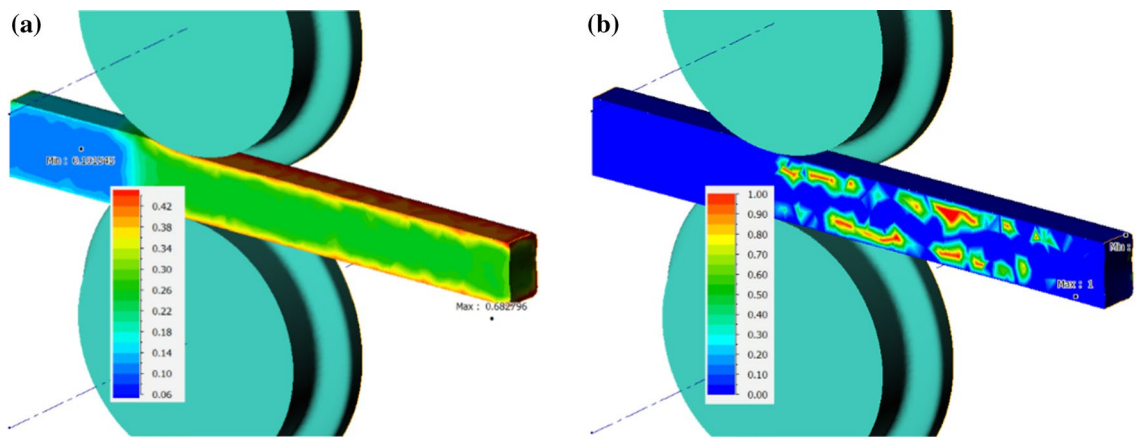
Fig. 10 Distribution of the critical strain (**a**) and recrystallized volume fraction (**b**) in the 3rd pass for bainitic steel

mechanical properties models solved at each Gauss integration point of the FE mesh. Two sets of simulations were performed. In the first set, different end of rolling temperatures and times of the air cooling after rolling were considered. In the second set, the effect of the average pearlite transformation temperature was investigated. Results of the hot rolling simulations (Fig. 12) were an input data for the simulation of cooling. The effect of the austenite grain size on the kinetics of transformations was taken into account.

For the sake of the model presentation, only the effect of the finish rolling temperature and the temperature at which the rail head is immersed in the solution, were considered
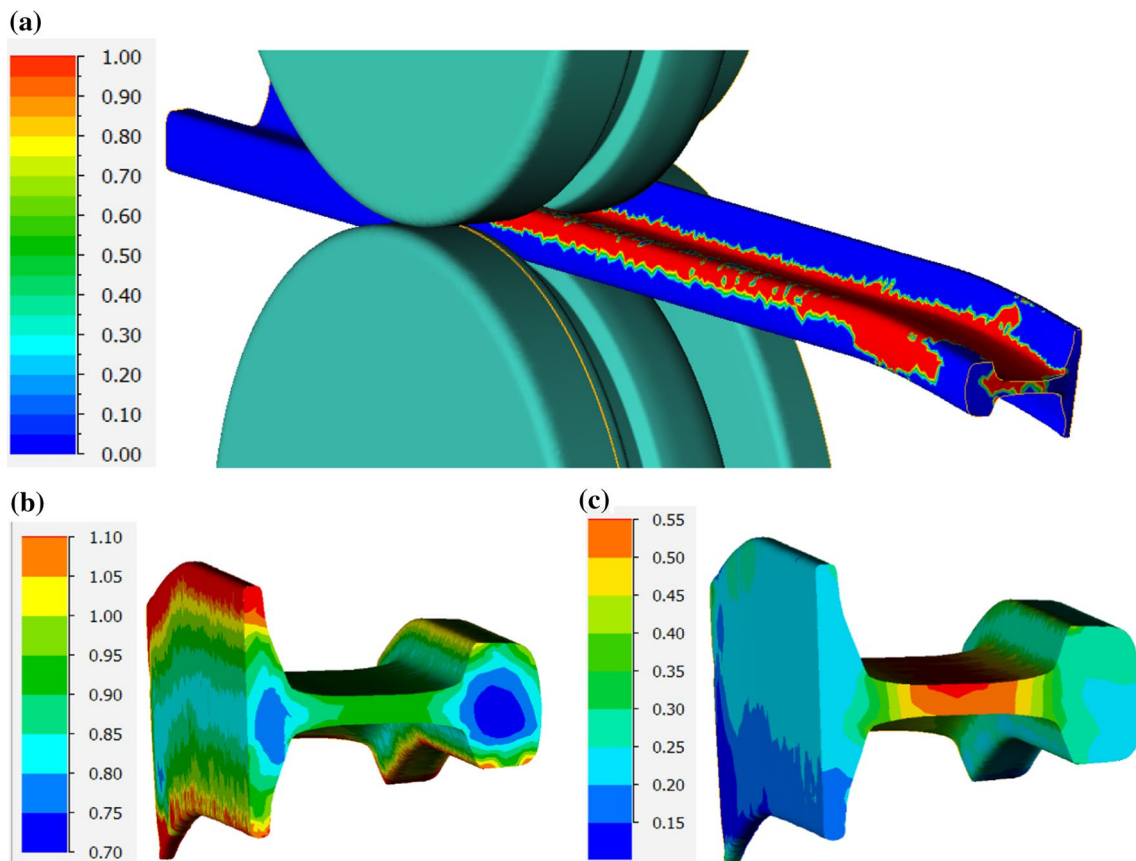
Fig. 11 Distribution of the recrystallized volume fraction (**a**) for pearlitic steel and critical strain (**b**) and effective strain (**c**) for bainitic steel in the last pass
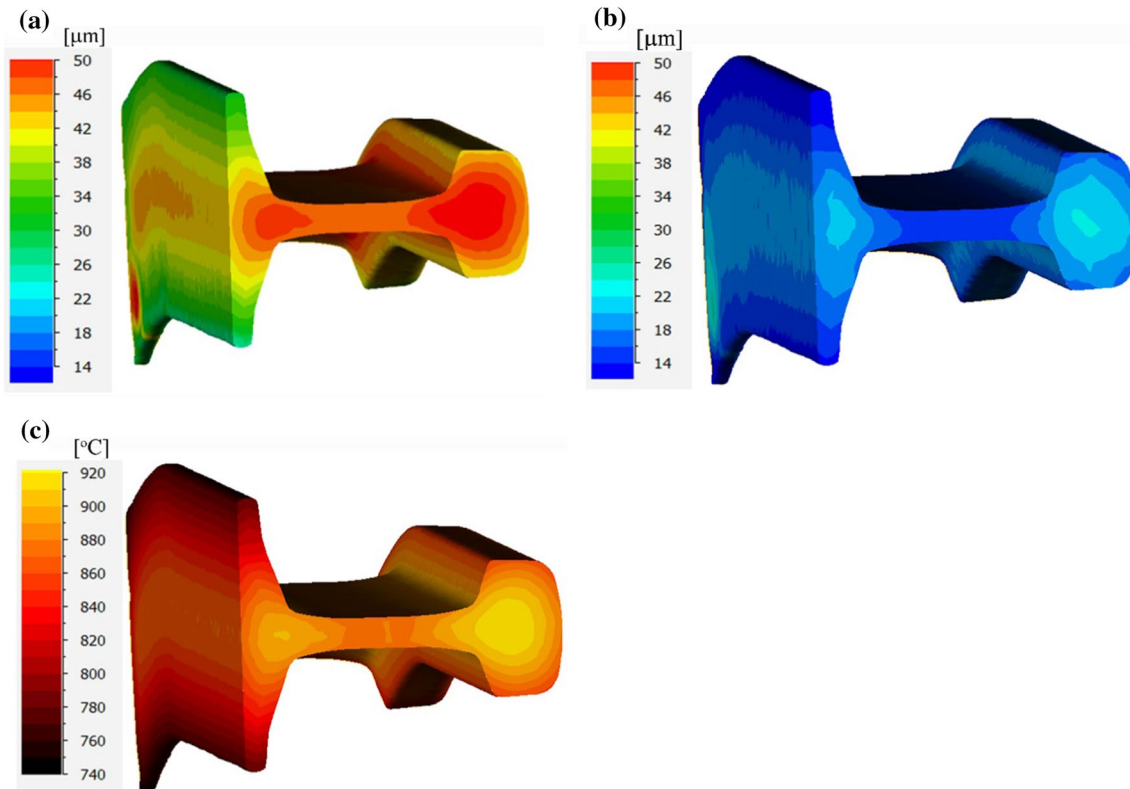
Fig. 12 Grain size distributions after hot rolling of the pearlitic (**a**) and bainitic (**b**) steel rails, μm; distribution of temperature in °C for both steels, time is 3 s after the last pass (**c**)

here. The analysis of the cyclic method of rails head hardening will be the subject of the subsequent paper. Three schedules were analyses in the first set of simulations. According to the schedule I, after cooling in the air to the temperature of 820 °C the rail head was immersed in the polymer solution. In the schedule II, the end of rolling temperature was decreased by 50 °C but the further cooling sequence was the same as in the schedule I. In the schedule III, the time of air cooling after rolling was longer and the temperature at the beginning of the immersion dropped to 720 °C. Times of cooling in the air after rolling were 98 s for the schedules I and II and 228 s for the schedule III. The time of the first immersion was 18 s for the schedules I and II and 7 s for the schedule III. The objective was to reach a similar surface temperature of about 600 °C for the schedules I and III after the immersion. Temperatures and phase compositions were analyzed at the 4 locations at the rail cross-section, as shown in Fig. 13a. For clearness of presentation, the results of time–temperature profiles and kinetics of transformation in Fig. 13b–d are shown for two points only: 2 mm from the head surface (A) and in the center of the rail head (C). The time scale for schedule II in Fig. 13b is moved to obtain the minimum temperature after the first immersion approximately at the same time. It can be concluded from Fig. 13c,d that the rate of the pearlite transformation is similar for all

schedules, however, the transformation occurs in different times.

The comparison of all parameters obtained for the points A and C after cooling according to the three schedules is presented in Table 8. Small difference between schedules I and III was observed. Only slightly finer microstructural parameters and higher mechanical properties close to the surface (point A) were obtained for the schedule I. Finer microstructure and higher mechanical properties were obtained for the finishing rolling temperature decreased by 50 °C (schedule II). The simulations show that the model is capable to predict microstructure and mechanical properties for rails cooled according to the complex thermal cycles.

To show the effect of the heat treatment, simulations for the schedule II were compared with the cooling in the air. Changes of temperature in four points are shown in Fig. 14a for the air cooling and in Fig. 14b for cooling in the solution. The effect of heating due to recalescence is seen for air cooling. This effect appears also during cooling in the solution but it is overwhelmed by a fast temperature drop. Results of calculation of the temperature of transformation, interlamellar spacing, hardness, and yield stress for these two cases are shown in Fig. 15. Cooling in the polymer solution results in the lower average temperature of transformation, finer interlamellar spacing, and higher mechanical properties.

Fig. 13 Locations of the sampling points (**a**), temperatures in the points A and C for the cooling schedules I, II and III (**b**) and kinetics of the pearlite transformation in the points A (**c**) and C (**d**)
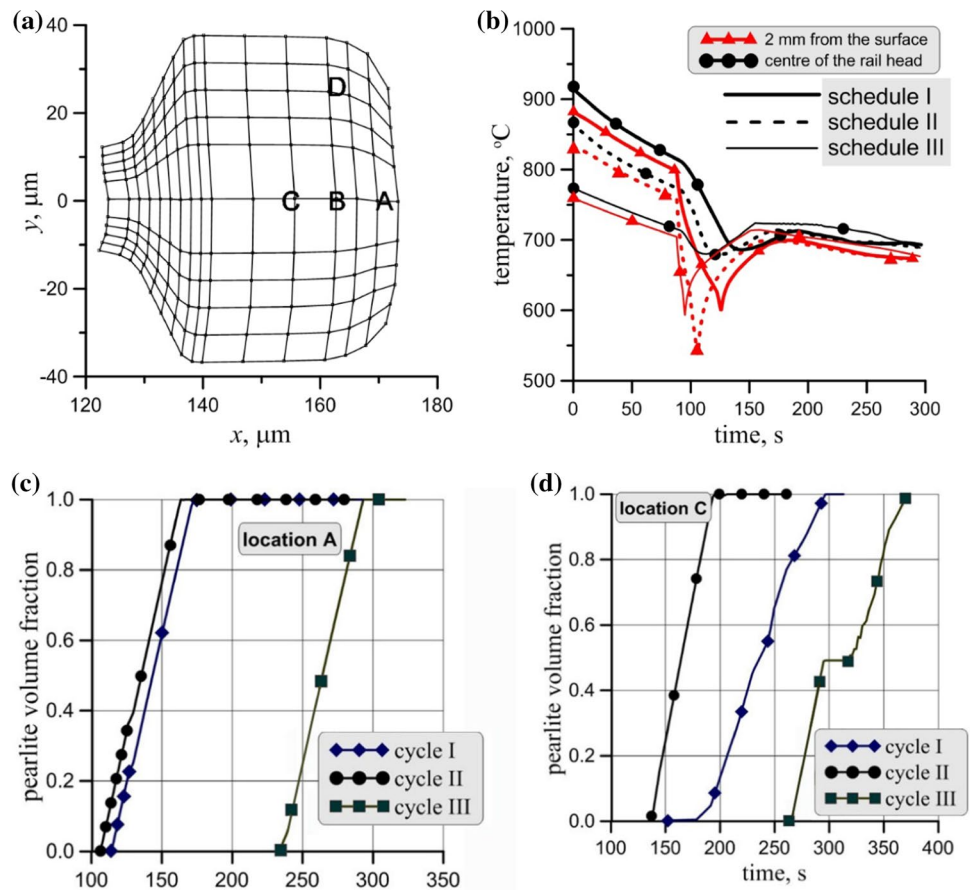
6.2 Pearlitic steels—effect of the end of cooling temperature

The goal of this set of simulations was to investigate the effect of time of the single immersion on the microstructure and properties of rails. To allow pearlite transformation to be completed during one immersion, the cooling time should be shorter compared to the laboratory experiments. Thus, the concentration of the polymer in the solution was assumed 10% what gave lower heat transfer coefficient, as follows: 1000 W/m^{2}K for temperatures exceeding 700 °C, increasing below this temperature and reaching 1440 W/m^{2}K at 300 °C,

decreasing below this temperature and dropping to 720 W/m^{2}K at the ambient temperature. Immersion times of 38 s, 44 s, 55, and 68 s were used to obtain minimum surface temperatures after immersion equal 600 °C, 560 °C, 520 °C, and 480 °C, respectively. Calculated parameters are presented in Fig. 16 as functions of the minimum temperature of the cycle. As could be expected, the decrease of the T_{min} leads to a decrease in the average transformation temperature, finer microstructure, and higher strength of the material. On the other hand, a certain amount of bainite was predicted in the area close to the surface for the lowest temperatures, example for $T_{min} = 480$ °C may be seen in Fig. 17, while

Table 8 Values of the parameters calculated in the two considered points

Location	T_p, °C	D_p, µm	D_c, µm	S_0, µm	σ_y, MPa	UTS, MPa	HV
A schedule I	650	62.7	13.2	0.126	646	1073	358
schedule II	612	40.1	8.3	0.11	704	1111	367
schedule III	659	86.9	18.7	0.137	617	1053	354
C schedule I	697	218.6	50.6	0.156	560	1006	347
schedule II	669	106.2	22.7	0.141	603	1044	352
schedule III	697	404.7	108.4	0.163	549	995	345

Fig. 14 Time-temperatures profiles at selected points for the cooling in the air (**a**) and for the cooling schedule II (**b**)
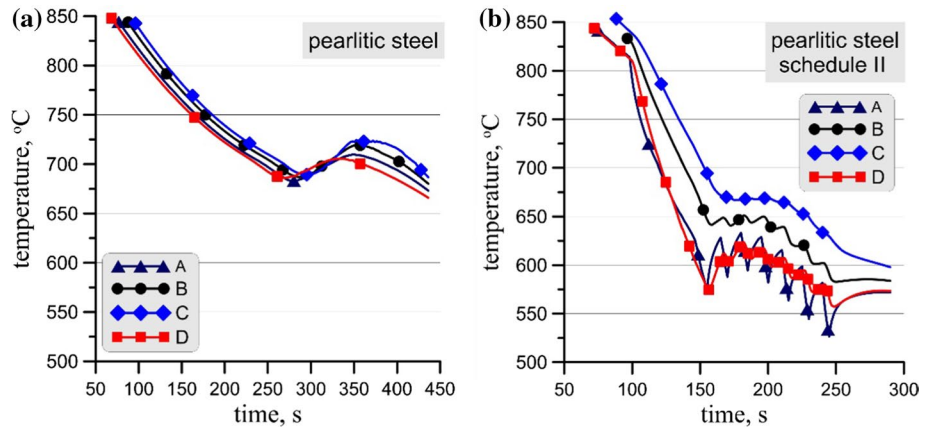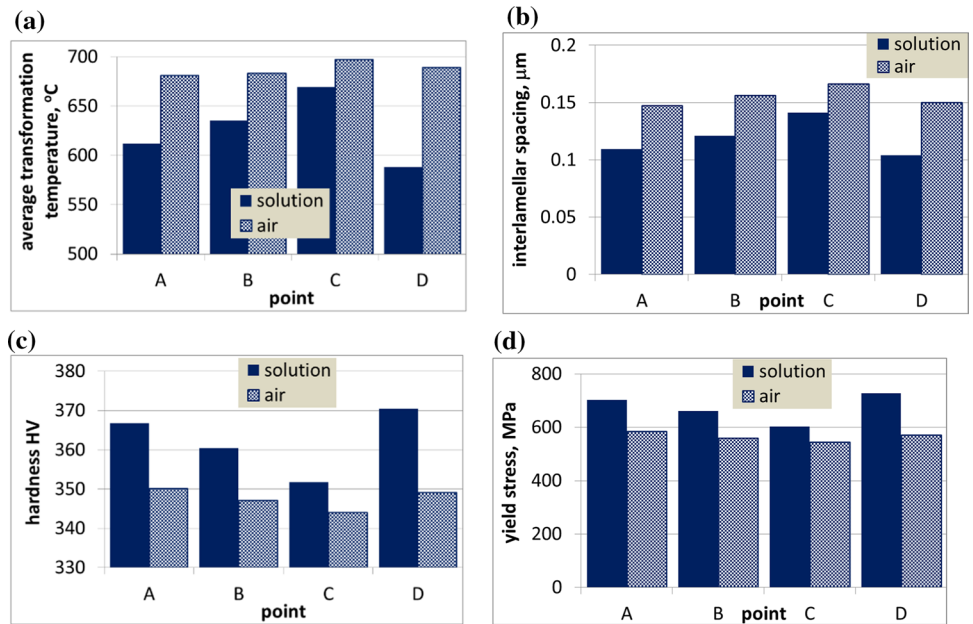

Fig. 15 The average temperature of the pearlitic transformation calculated from equation (15) (**a**), interlamellar spacing (**b**), hardness (**c**) and yield stress (**d**) at four locations shown in Fig. 13a—comparison of the cooling in the air and following the schedule I in Fig. 13b

almost purely pearlitic microstructure was predicted for the remaining temperatures.

Numerical tests confirmed good predictive capabilities of the model. Simulations have shown that it is possible to predict the optimal time of the immersion for the specific concentration of the polymer in the solution accounting for the end of rolling temperature.

6.3 Bainitic steels

Cooling of bainitic steel in the air was simulated. The bainitic microstructure was obtained for both steels at the whole cross-section of the rail. To investigate the sensitivity of the model to changes in the cooling rate, additional simulations were performed. Forced convection with the air velocity of 3 m/s was considered to test faster cooling. Decreased

emissivity to 0.4 was assumed to simulate slow cooling. The results of simulations are presented in Fig. 18 for the point A in Fig. 13a. It is seen that slightly faster bainitic transformation was obtained for the steel B. Faster cooling resulted in about 7% of the martensite in this steel. Purely bainitic microstructure (below 3% of ferrite) was obtained for the steel A.

Properties of the rail head were calculated from equations presented earlier in the paper. Due to the low level of microalloying +, the effect of precipitation was calculated for a very low volume fraction of precipitates and it was at the level of 50 MPa. Calculated distribution of the yield strength and ultimate tensile strength in the rail head is shown in Fig. 19. Elongation calculated from the equation (25) was uniform in the whole rail head and was $A_5 = 13\%$ for steel A and $A_5 = 17\%$ for steel B. Predicted

Fig. 16 The effect of the minimum temperature in the cycle on the average temperature of pearlite transformation, yield stress and ultimate tensile strength (**a**) and on the interlamellar spacing and colony size (**b**), for the location A (solid lines) and the location C (dashed lines)
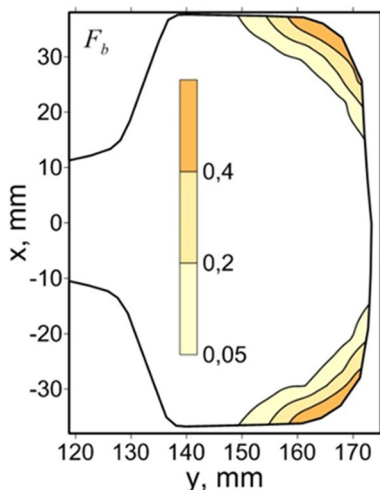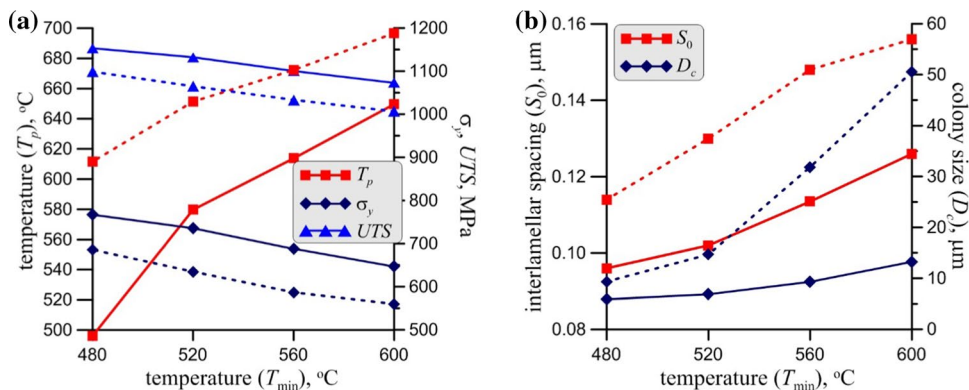

Fig. 17 Distribution of the bainite volume fraction for the $T_{min} = 480\ °C$

mechanical properties of bainitic steels were compared with measurements presented in Table 9 and good agreement was obtained.

7 Conclusions

FE simulation with microstructure evolution equation solved at each node of the FE mesh allowed to predict mechanical, thermal, and metallurgical parameters during hot rolling and supplied a new transferrable knowledge on the rail rolling process. Results of the hot rolling simulations, i.e., temperature and austenite distribution at the cross-section of the rail are the input data to the model of phase transformation during cooling. Moreover, numerical tests and optimization of the cooling process allowed to formulate the following conclusions:

1. For rolling:
a. In the last pass, partial dynamic recrystallization for the pearlitic steel was observed. But the dominant mechanism of recrystallization was static. For bainitic steel, the value of the critical strain exceeded the effective strain and dynamic recrystallization did not start. Static recrystallization only was observed.
b. Modelling of the mechanisms of recrystallization (dynamic and static) showed that for pearlitic steel the

Fig. 18 Calculated temperatures and kinetics of transformations during cooling with various cooling rates of the bainitic steel A (**a**) and B (**b**) (the meaning of lines and symbols is the same in both plots)
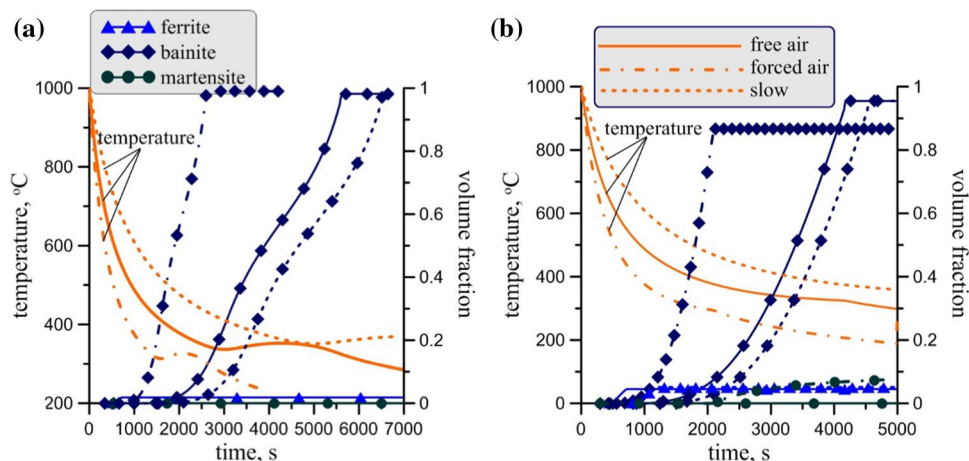
Fig. 19 Calculated distribution of the yield strength (**a,c**) and ultimate tensile strength (**b,d**) in the rail head for the steel A (**a,b**) and B (**c,d**)
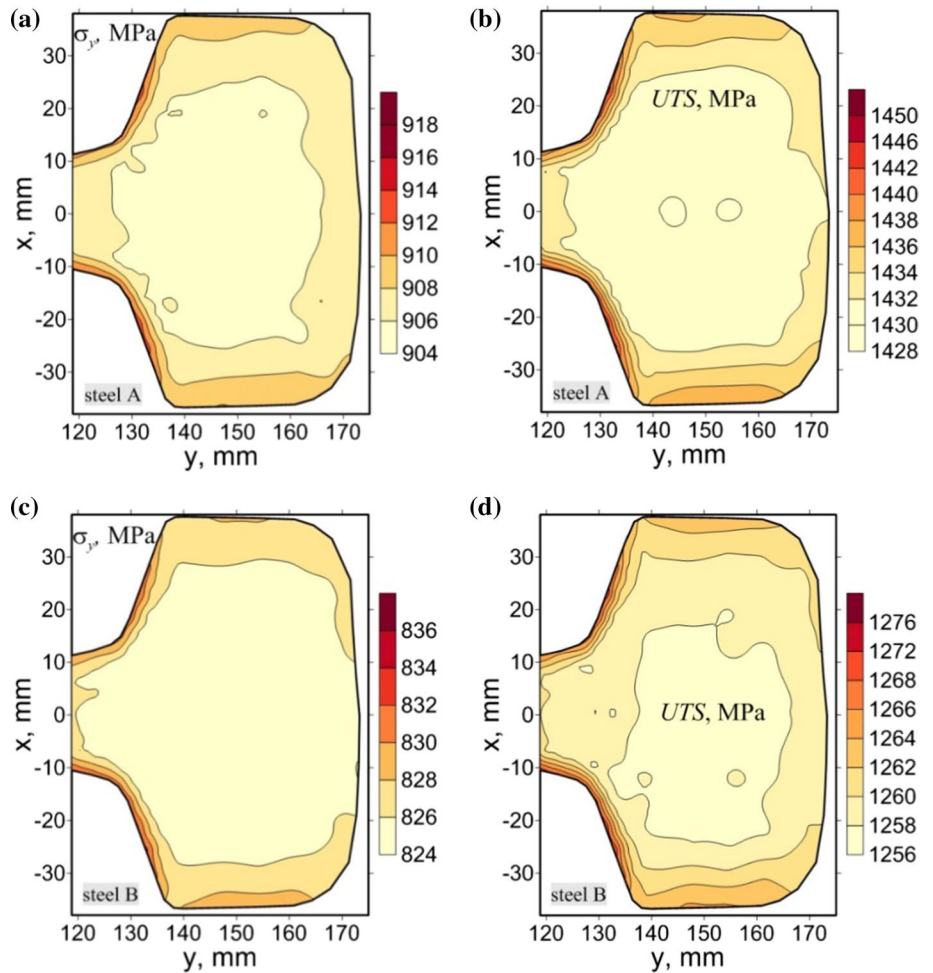

Table 9 Measured mechanical properties of bainitic steels

Material	σ_y, MPa	UTS, MPa	A_5, %	Z, %	KV, J	
					+ 20 °C	− 20 °C
Steel A	962	1497	14.5	42.2	27.5	23.0
Steel B	820	1276	16.3	36.4	15.5	10.0

recrystallization is much faster than for bainitic steel. However, in 1.5 s after the last pass, the recrystallization of both steels was completed.

c. The results show that pearlitic steel has larger grains than bainitic steel. The distribution of grain diameter is more uniform for bainitic steel.

2. For cooling:

a. Numerical tests confirmed good predictive capabilities of the model as far as the kinetics of transformation and product properties are considered.

b. The effect of the time of air cooling after rolling is negligible when the temperatures after the first immersion are the same.

c. The heat transfer coefficient has the strongest effect on the optimization results. HTC can be controlled by changing the concentration of the polymer.

d. The time of the first immersion has a strong effect on the properties of products. This time determines the average transformation temperature and, in consequence, it influences microstructural parameters and mechanical properties.

e. Simulations have shown that it is possible to predict the optimal time of the immersion for the specific concentration of the polymer in the solution, accounting for the end of rolling temperature.

References

1. Kuziak R, Zygmunt T. A new method of rail head hardening of standard-gauge rails for improved wear and damage resistance. Steel Res Int. 2013;84:13–9.
2. Bhadeshia HKDH. Novel steels for rails. In: Buschow K, Cahn RW, Flemings MC, Iischner B, Kramer EJ, Mahajan S, editors. Encyclopedia of materials science: science and technology. Oxford: Pergamon Press; 2002. p. 1–7.
3. Zajac S, Schwinn V, Tacke KH. Characterisation and quantification of complex bainitic microstructures in high and ultra-high strength linepipe steels. Mater Sci Forum. 2005;500–501:387–94.
4. Hiramatsu H, Egashira T, Yuta K, Nakamata S. Temperature distribution of structural sections during hot rolling. Tetsu-to-Hagane. 1970;56:1891–8 **(in Japanese)**.
5. Gołdasz A, Malinowski Z, Hadała B, Rywotycki M. Influence of the radiation shield on the temperature of rails rolled in the reversing mill. Arch Metall Mater. 2015;60:275–9.
6. Głowacki M. Simulation of rail rolling using the generalized plane-strain finite-element approach. J Mater Process Technol. 1996;62:229–34.
7. Głowacki M, Kuziak R, Malinowski Z, Pietrzyk M. Modelling of heat transfer, plastic flow and microstructural evolution during shape rolling. J Mater Process Technol. 1995;53:159–66.
8. Głowacki M. The mathematical modelling of thermo-mechanical processing of steel during multi-pass shape rolling. J Mater Process Technol. 2005;168:336–43.
9. Lindback TE, Nasstrom M. Residual stresses in railway rails after manufacturing. In: Mori K, editor. Proceedings of Conference NUMIFORM, Toyohashi, 2001; pp. 567–576.
10. Guerrero MA, Belzunce J, Betegón MC, Jorge J, Vigil FJ. Hot rolling process simulation. Application to UIC-60 rail rolling, Proceedings of the 4th IASME/WSEAS International Conference on Continuum Mechanics, Cambridge, 2009; pp. 213–218.
11. Janiyani SG, Solanki PD. Simulation of roll passes for section rolling of flat-footed rail section with the help of FEA. Int J Eng Res Technol. 2012;1:1–6.
12. Kim SY, Im Y-T. Three dimensional finite element analysis of non-isothermal shape rolling. J Mater Process Technol. 2002;127:57–63.
13. Altınkaya H, Orak IM, Esen I. Artificial neural network application for modeling the rail rolling process. Expert Syst Appl. 2014;41:7135–46.
14. Sahay SS, Mohapatra G, Totten GE. Overview of pearlitic rail steels: accelerated cooling, quenching, microstructure and mechanical properties. J ASTM Int. 2009;6:1–26.
15. Perez-Unzueta AJ, Beynon JH. Microstructure and wear resistance of pearlitic rail steels. Wear. 1993;162–164:173–82.
16. Szeliga D, Kuziak R, Zygmunt T, Kusiak J, Pietrzyk M. Selection of parameters of the heat treatment thermal cycle for rails with respect to the wear resistance. Steel Res Int. 2014;85:1070–82.
17. Boyadiev II, Thomson PF, Lam YC. Computation of the diffusional transformation of continuously cooled austenite for predicting the coefficient of thermal expansion in the numerical analysis of thermal stress. ISIJ Int. 1996;36:1413–9.
18. Lee K-M, Polycarpou AA. Microscale experimental and modelling wear studies of rail steels. Wear. 2011;271:1174–80.
19. Kuziak R, Cheng Y-W, Głowacki M, Pietrzyk M. Modelling of the microstructure and mechanical properties of steels during thermomechanical processing, NIST Technical Note 1393, Boulder, 1997.
20. Kuziak R, Pidvysots'kyy V, Pernach M, Rauch Ł, Zygmunt T, Pietrzyk M. Strategy based on physical simulations for the selection of the best phase transformation model for optimization of manufacturing processes of pearlitic steel rails. Arch Civ Mech Eng. 2019;19:535–46.
21. Kobayashi S, Oh SI, Altan T. Metal forming and the finite element method. New York: Oxford University Press; 1989.
22. Pietrzyk M. Finite element simulation of large plastic deformation. J Mater Process Technol. 2000;106:223–9.
23. Sellars CM. Physical metallurgy of hot working. In: Sellars CM, Davies GJ, editors. Hot working and forming processes. London: The Metals Society; 1979. p. 3–15.
24. Pietrzyk M, Kuziak R. Modelling phase transformations in steel. In: Lin J, Balint D, Pietrzyk M, editors. Microstructure evolution in metal forming processes. Oxford: Woodhead Publishing; 2012. p. 145–179.
25. Pietrzyk M, Madej Ł, Rauch Ł, Szeliga D. Computational materials engineering: achieving high accuracy and efficiency in metals processing simulations. Amsterdam: Elsevier; 2015.
26. Bhadeshia HKDH. Bainite in steels. 2nd ed. London: IOM Communications; 2002.
27. Katsamas AI, Haidemenopoulos GN. A semi–empirical model for the evolution of retained austenite via bainitic transformation in multiphase TRIP steels. Steel Res Int. 2008;79:875–84.
28. Pietrzyk M., Kania Z., Kuziak R., Rauch Ł., Kusiak J., A simple model for prediction of retained austenite in steel rods after hot rolling and controlled cooling.In: Buchmayr B., Zauchensee, editors. Proceedings of XXXV Verformungskundliches Kolloquium. 2016; 56–66.
29. Zajac S, Komenda J, Morris P, Matera S, Penalba DF. Quantitative structure-property relationships for complex bainitic microstructure, RFCS Final Report, European Commission, Luxembourg, 2003.
30. Halfa H. Recent trends in producing ultrafine grained steels. J Miner Mater Character Eng. 2014;2:428–69.

31. Morrison W. The effect of grain size on the stress-strain relationship in low carbon Steel. Trans Am Soc Metals. 1996;59:824–46.

32. Brozzo P, Buzzichelli A, Mascanzoni A, Mirabile G. Microstructure and cleavage resistance of low carbon bainitic steel. Metal Sci. 1977;11:123–30.

33. Bhadeshia H. Steels. Microstructure and properties, 3rd ed., Elsevier, Butterworth-Heinemann, Amsterdam, 2006.

34. Takahashi M, Bhadeshia H. Model for transition from upper to lower bainite. Mater Sci Technol. 1990;6:592–603.

35. Szeliga D, Gawąd J, Pietrzyk M. Inverse analysis for identification of rheological and friction models in metal forming. Comput Methods Appl Mech Eng. 2006;195:6778–98.

36. Lenard JG, Pietrzyk M, Cser L. Mathematical and physical simulation of the properties of hot rolled products. Amsterdam: Elsevier; 1999.